Rigid, Complete Annuloplasty Rings Increase Anterior Mitral Leaflet Strains in the Normal Beating Ovine Heart

Wolfgang Bothe, MD; Ellen Kuhl, PhD; John-Peder Escobar Kvitting, MD, PhD; Manuel K. Rausch, MSc; Serdar Göktepe, PhD; Julia C. Swanson, MD; Saideh Farahmandnia, MD; Neil B. Ingels, Jr, PhD; D. Craig Miller, MD

Background**—**Annuloplasty ring or band implantation during surgical mitral valve repair perturbs mitral annular dimensions, dynamics, and shape, which have been associated with changes in anterior mitral leaflet (AML) strain patterns and suboptimal long-term repair durability. We hypothesized that rigid rings with nonphysiological three-dimensional shapes, but not saddle-shaped rigid rings or flexible bands, increase AML strains.

Methods and Results**—**Sheep had 23 radiopaque markers inserted: 7 along the anterior mitral annulus and 16 equally spaced on the AML. True-sized Cosgrove-Edwards flexible, partial band (n=12), rigid, complete St Jude Medical rigid saddle-shaped (n=12), Carpentier-Edwards Physio (n=12), Edwards IMR ETlogix (n=11), and Edwards GeoForm (n=12) annuloplasty rings were implanted in a releasable fashion. Under acute open-chest conditions, 4-dimensional marker coordinates were obtained using biplane videofluoroscopy along with hemodynamic parameters with the ring inserted and after release. Marker coordinates were triangulated, and the largest maximum principal AML strains were determined during isovolumetric relaxation. No relevant changes in hemodynamics occurred. Compared with the respective control state, strains increased significantly with rigid saddle-shaped annuloplasty ring, Carpentier-Edwards Physio, Edwards IMR ETlogix, and Edwards GeoForm (0.14±0.05 versus 0.16±0.05, P=0.024, 0.15±0.03 versus 0.18±0.04, P=0.020, 0.11±0.05 versus 0.14±0.05, P=0.042, and 0.13±0.05 versus 0.16±0.05, P=0.009), but not with Cosgrove-Edwards band (0.15±0.05 versus 0.15±0.04, P=0.973).

Conclusions**—**Regardless of three-dimensional shape, rigid, complete annuloplasty rings, but not a flexible, partial band, increased AML strains in the normal beating ovine heart. Clinical studies are needed to determine whether annuloplasty rings affect AML strains in patients, and, if so, whether ring-induced perturbations in leaflet strain states are linked to repair failure. **(*Circulation*. 2011;124[suppl 1]:S81–S96.)**

Key Words: mitral valve ■ physiology ■ mitral valve insufficiency ■ general surgery

Surgical mitral valve repair most commonly includes the insertion of an annuloplasty band or ring. Whereas bands are flexible devices that spare the anterior, fibrous portion of the mitral annulus, rings encircle the entire annulus and may be flexible, semirigid, or rigid. Rigid rings are available in various shapes. The most commonly used ring (Carpentier-Edwards Physio [PHYSIO]) is flat, semirigid, and D-shaped. Recently, saddle-shaped, rigid, complete annuloplasty rings have been introduced (eg, Saint Jude Medical rigid saddle-shaped annuloplasty ring [RSAR], Medtronic Profile 3-D, and PHYSIO II) to account for the physiological three-dimensional (3D) shape of the mitral annulus.[1,2] Furthermore, rigid rings with nonphysiological shapes and dimensions have been designed specifically for patients with functional/ischemic mitral regurgitation (eg, Edwards GeoForm [GEO] and IMR ETlogix [ETL]). These rings aim to counteract the main determinants of functional/ischemic mitral regurgitation (ie, mitral annular dilatation, left ventricular dilatation and papillary muscle displacement) on an annular level via their specific designs, all of which include disproportionate annular septal-lateral (S-L) downsizing.[3] Although some studies demonstrate that such rings may reduce mitral leaflet strains in the diseased heart,[4] other studies suggest that, by perturbing the natural saddle-shaped mitral annulus, disease-specific or nonphysiologically shaped rings may increase leaflet strains in the normal heart.[5–7] Because of these results from in vitro measurements, it has been speculated that such perturbations in mitral leaflet strain patterns could be associated with impaired long-term results after mitral valve repair.[5–7] Our goal, therefore, was to assess the effects of 1 flexible, partial band and 4 different complete annuloplasty rings on anterior mitral leaflet (AML) strains in healthy, beating ovine

From the Department of Cardiothoracic Surgery (W.B., E.K., J.-P.E.K., J.C.S., S.F., N.B.I., D.C.M.), Stanford University School of Medicine, Stanford, CA; Department of Mechanical Engineering (M.K.R., S.G.), Stanford University School of Engineering, Stanford, CA; Laboratory of Cardiovascular Physiology and Biophysics (N.B.I.), Research Institute, Palo Alto Medical Foundation, Palo Alto, CA.

Presented at the 2010 American Heart Association meeting in Chicago, IL, November 12–16, 2010.

Correspondence to D. Craig Miller, MD, Department of Cardiothoracic Surgery, Falk Cardiovascular Research Center, Stanford University School of Medicine, Stanford, CA 94305-5247. E-mail dcm@stanford.edu

Circulation **is available at http://circ.ahajournals.org** **DOI: 10.1161/CIRCULATIONAHA.110.011163**

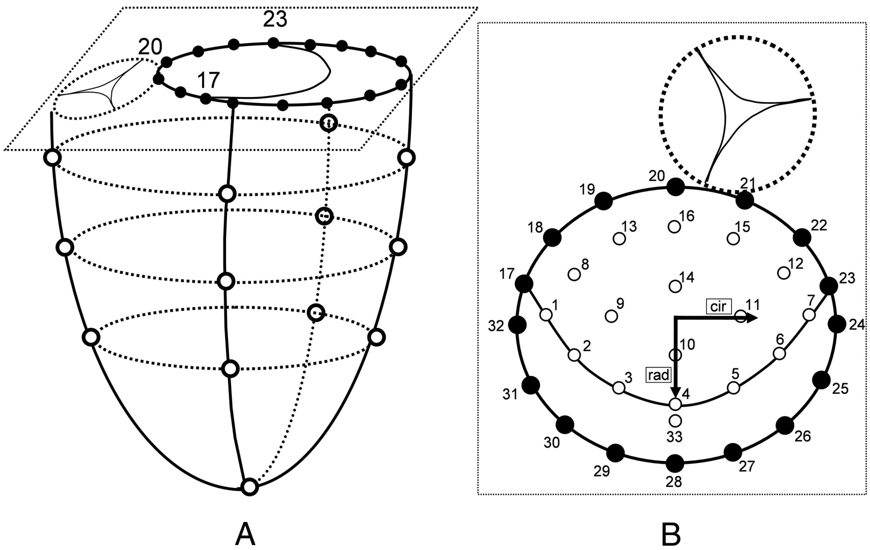

Figure 1. A, Schematic illustrating ventricular and annular marker locations. Marker 20 represents the mitral annular saddle horn marker, and markers 17 and 23 represent the anterior and posterior commissural markers, respectively. **B**, Schematic magnification of a top view of the mitral valve showing annular as well as leaflet markers. Sixteen markers were placed on the mitral annulus (markers 17 to 32), 16 markers were placed on the anterior mitral leaflet (AML) (markers 1 to 16), and 1 marker was placed on the free edge of the mid-part of the posterior leaflet (marker 33). Inset shows the radial (rad) and circumferential (cir) directions used for strain definitions.

hearts. We tested the hypothesis that rigid, complete rings with nonphysiological 3D shapes, but not saddle-shaped rigid rings or flexible, partial bands, increase maximum principal strains across the AML.

Methods

All animals received humane care in compliance with the *Principles of Laboratory Animal Care* formulated by the National Society for Medical Research and the *Guide for Care and Use of Laboratory Animals* prepared by the National Academy of Sciences and published by the National Institutes of Health (Department of Health Education and Welfare Publication 85-23, revised 1985). This study was approved by the Stanford Medical Center Laboratory Research Animal Review Committee and was conducted according to Stanford Universitypolicy.

Surgical Preparation

Fifty-nine adult, Dorsett-hybrid, male sheep (49±5 kg) were premedicated with ketamine (25 mg/kg intramuscularly), anesthetized with sodium thiopental (6.8 mg/kg intravenously), intubated, and mechanically ventilated with inhalational isoflurane (1.0% to 2.5%). A left thoracotomy was performed, and the heart was suspended in a pericardial cradle. Thirteen miniature radiopaque tantalum markers were surgically implanted into the subepicardium to silhouette the left ventricular chamber at the intersections of 2 longitudinal and 3 crosswise meridians, as shown in Figure 1A. Using cardiopulmonary bypass and cardioplegic arrest, a total of 33 radiopaque tantalum markers were sewn to the following sites (Figure 1B): 16 around the mitral annulus (markers 17 to 32, Figure 2A and 2B), 16 equally spaced on the atrial aspect of the AML (markers 1 to 16, Figure 2B), and 1 on the central edge of the middle scallop of the posterior mitral leaflet (marker 33, Figure 2B). A single tantalum loop (0.6 mm inner diameter, 1.1 mm outer diameter, 3.2 mg) was used for each leaflet marker.

After marker placement, 5 different annuloplasty ring models, the Cosgrove-Edwards band (COS) (Edwards Lifesciences, Irvine, CA, USA, n=12), RSAR (St. Jude Medical Inc, St. Paul, MN, n=12), PHYSIO (n=12), Edwards IMR ETL (n=11), and Edwards GeoForm (GEO, n=12, all three Edwards Lifesciences, Irvine, CA) were implanted in a releasable fashion as described earlier.[8] In brief, the annuloplasty devices were prepared before the operation in the following manner: the middle parts of 8 double-armed polyester braided sutures were stitched evenly spaced around the ring or band from the bottom to the top side using a "spring eye" needle. The resulting loops were "locked" with 2 polypropylene sutures. The polyester sutures were stitched equidistantly in a perpendicular direction from the ventricular to the atrial side through the mitral annulus. The annuloplasty devices were secured to the mitral annulus by tying these sutures. The locking sutures (polypropylene) and the drawstrings were exteriorized before the atrium was closed. Ring and band sizes were determined by assessing the entire area of the AML

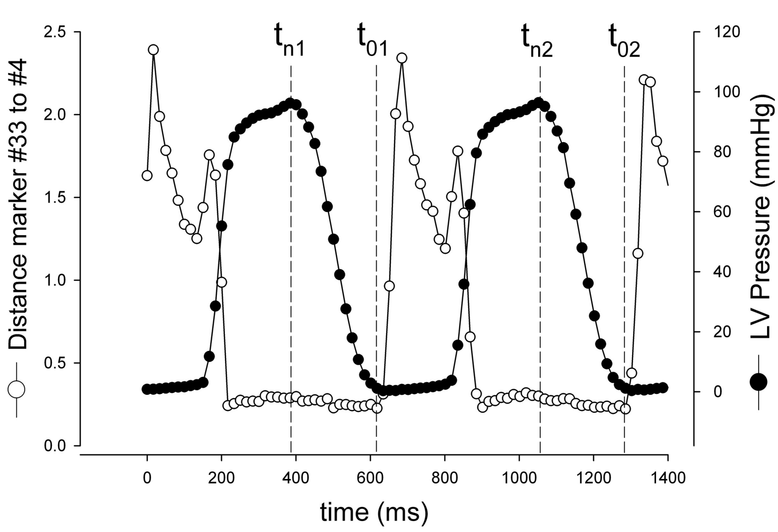

Figure 2. Illustration of time point definitions. Time point t_n (strained state) was defined as maximum left ventricular (LV) pressure for beat 1 (t_{n1}) and beat 2 (t_{n2}). Time point t_0 (reference state) was defined as last time frame before mitral leaflet separation (as represented by the rapid increase in plotted curve of distances (cm) between markers 33 and 4; see Figure 1) for beat 1 (t_{01}) and beat 2 (t_{02}).

Table 1. Heart Rate, Left Ventricular End-Diastolic Volume, and dP/dt_{max}

	Animal No													Mean±1 SD				
	1	2	3	4	5	6	7	8	9	10	11	12	HR (min^{-1})	*P* vs CTRL	LVEDV (mL)	*P* vs CTRL	dP/dt_{max} (mm Hg)	*P* vs CTRL
COS-CTRL																		
HR (min^{-1})	89	104	124	103	87	76	114	90	100	113	85	94	98±14					
LVEDV (mL)	109	104	107	137	136	111	132	100	113	122	149	122			120±15			
dP/dt_{max} (mm Hg)	979	1619	1289	1069	1853	1514	1742	1238	1478	1564	846	1128					1360±317	
COS																		
HR (min^{-1})	97	111	118	101	87	73	114	90	97	111	86	94	98±13	0.914				
LVEDV (mL)	109	100	118	139	137	117	132	100	111	122	149	119			121±16	0.392		
dP/dt_{max} (mm Hg)	1280	1905	1309	1100	2018	1635	2196	1294	1739	1636	970	1240					1527±386	0.001
RSAR-CTRL																		
HR (min^{-1})	74	122	113	94	71	88	88	86	106	66	87	77	89±17					
LVEDV (mL)	91	80	135	100	122	112	140	156	113	136	123	138			121±22			
dP/dt_{max} (mm Hg)	1309	2296	1267	1109	1055	1794	1082	1381	1039	1232	708	1125					1283±409	
RSAR																		
HR (min^{-1})	77	113	114	96	73	90	89	85	104	67	85	74	89±15	0.853				
LVEDV (mL)	96	85	139	103	124	110	138	149	111	133	123	140			121±20	0.714		
dP/dt_{max} (mm Hg)	1202	1817	1313	1312	1145	1692	1131	1011	1087	1111	682	1212					1226±297	0.340
PHYSIO-CTRL																		
HR (min^{-1})	84	118	107	80	99	84	88	82	88	100	87	90	92±12					
LVEDV (mL)	174	136	112	136	126	87	124	119	99	126	120	128			124±21			
dP/dt_{max} (mm Hg)	1694	1187	1307	841	1343	1551	1014	1116	1948	1239	888	1560					1307±333	
PHYSIO																		
HR (min^{-1})	84	111	107	78	103	83	88	82	91	99	88	88	92±11	0.517				
LVEDV (mL)	178	138	118	139	116	80	125	118	96	128	123	128			124±24	0.934		
dP/dt_{max} (mm Hg)	1896	1186	1290	835	1683	1757	1166	1056	1426	1362	913	1606					1348±337	0.523
ETL-CTRL																		
HR (min^{-1})	87	79	85	76	76	79	78	80	91	94	74		82±6					
LVEDV (mL)	145	105	96	147	115	94	120	140	125	148	139				125±20			
dP/dt_{max} (mm Hg)	1879	681	1630	1064	1091	1348	1085	821	728	1322	1207						1169±368	
ETL																		
HR (min^{-1})	60	79	83	81	75	80	78	83	91	96	74		80±9	0.531				
LVEDV (mL)	150	104	96	147	120	98	117	139	123	145	137				125±20	0.833		
dP/dt_{max} (mm Hg)	1860	686	1591	1053	1098	1399	1073	874	772	1492	1188						1190±363	0.259
GEO-CTRL																		
HR (min^{-1})	80	82	94	100	96	106	106	86	85	106	84	82	92±10					
LVEDV (mL)	89	113	120	114	122	131	131	107	113	95	109	130			114±13			
dP/dt_{max} (mm Hg)	1030	1238	1298	1248	1469	1043	1163	1392	1138	1342	2221	1180					1313±315	
GEO																		
HR (min^{-1})	83	79	95	103	97	104	109	91	99	96	84	79	93±10	0.492				
LVEDV (mL)	89	116	119	105	119	130	129	101	107	104	106	129			113±13	0.223		
dP/dt_{max} (mm Hg)	1070	1259	1398	1144	1569	1181	1372	1509	1110	1321	2586	1131					1388±41	0.070

All values from individual animals are 2-beat averages. COS indicates Cosgrove-Edwards band; CTRL, control; ETL, Edwards IMR ETlogix; GEO, Edwards GeoForm; HR, heart rate; LVEDV, left ventricular end-diastolic volume; PHYSIO, Carpentier-Edwards Physio; RSAR, Saint Jude Medical rigid saddle-shaped annuloplasty ring.

using a sizer from Edwards Lifesciences. All annuloplasty devices were true-sized (as all animals had similarly sized leaflets, each received size 28 rings or bands). The left atrium was closed, and the left circumflex artery was encircled with a vessel loop for a parallel study.[9] Data from mitral annular and leaflet geometry using this data set have been published earlier.[8–11] The animals were then transferred to the experimental catheterization laboratory for data acquisition under acute open-chest conditions.

Data Acquisition

Videofluoroscopic images (60 frames/s) of all radiopaque markers were acquired using biplane videofluoroscopy (Philips Medical Systems, Pleasanton, CA). First, images were acquired under baseline conditions with the ring inserted (COS, RSAR, PHYSIO, ETL, GEO). Following the data acquisition under baseline conditions, 90 seconds of ischemia was induced, for a parallel study, by tightening the encircling left circumflex artery vessel loop with a tourniquet. Thereafter, the locking sutures were pulled out, and the ring was lifted away from the mitral annulus toward the left atrial roof using the drawstrings. After hemodynamic values returned to baseline, a third data acquisition was performed, and images were acquired under baseline conditions with the ring released (COS-control [CTRL], RSAR-CTRL, PHYSIO-CTRL, ETL-CTRL, GEO-CTRL). Marker coordinates from 2 consecutive sinus rhythm heart beats from each of the biplane views were then digitized and merged to yield the 3D coordinates of each marker centroid in each frame using semiautomated image processing and digitization software.[12] Simultaneously, analog left ventricular pressures (LVP), as well as ECG signals, were recorded in real time on the video images during data acquisition.

Hemodynamic Parameters and Cardiac Cycle Timing

For each beat, the end-diastolic videofluoroscopic frame was defined as the frame that coincided with the peak of the R-wave on the ECG. To calculate leaflet strains, a reference configuration during diastole and a deformed configuration during peak systole were determined for each beat (t_0 and t_n, respectively, Figure 2). When defining these configurations, the goal was to quantify strains with the mitral valve closed in both configurations and maximize the LVP difference between the 2 time points. To identify the reference configuration, the distance between AML central edge (marker 4, Figure 1B) and posterior mitral leaflet edge marker (marker 33, Figure 1B) was plotted throughout the cardiac cycle for each animal. For each heartbeat, the time point of leaflet opening was defined as the time point immediately before the AML and posterior mitral leaflet started to separate (Figure 2), thereby defining the reference state for beat 1 (t_{01}, Figure 2) and beat 2 (t_{02}, Figure 2). To identify the deformed configuration, LVP curves were plotted throughout the cardiac cycle. The time point of maximum LVP for each heartbeat was defined as the deformed state (t_{n1} and t_{n2}, respectively, Figure 2). The embedded period between these 2 states closely reflects the period of isovolumetric relaxation (Figure 2). Maximum systolic dP/dt (dP/dt_{max}) was calculated for each beat for each animal. Left ventricular volumes (LVV) were calculated from space-filling tetrahedral fit between all left ventricular markers at each beat at end-diastole (left ventricular end-diastolic volume), t_{n1}, t_{n2}, t_{01}, and t_{02} (see Moon et al[13] for details). Changes in LVP and LVV (Δ_{LVP} and Δ_{LVV}, respectively) from t_{01} to t_{n1} and from t_{02} to t_{n2} were calculated as $LVPt_{n1}-LVPt_{01}$ and $LVPt_{n2}-LVPt_{02}$ and as $LVVt_{n1}-LVVt_{01}$ and $LVVt_{n2}-LVVt_{02}$, respectively.

Mitral Annular Dimensions

At t_{n1}, t_{n2}, t_{01}, and t_{02}, distances between markers 20 and 28 and distances between markers 32 and 24 (Figure 1B) were calculated to determine S-L and commissure-commissure (C-C) annular dimensions, respectively. Changes in mitral annular S-L and C-C dimensions ($\Delta_{S\text{-}L}$ and $\Delta_{C\text{-}C}$, respectively) from t_{01} to t_{n1} and from t_{02} to t_{n2} were calculated as $t_{n1}-t_{01}$ and $t_{n2}-t_{02}$.

Global Maximum Principal, Radial, and Circumferential Strains

To determine the largest (global) maximum principal, radial and circumferential strains across the entire leaflet, the 16 AML mitral leaflet markers (markers 1 to 16, Figure 1B) and the 7 mitral annular markers (markers 17 to 23, Figure 1B) were triangulated, and 30 triangular membrane elements were generated. For each triangle, the co- and contravariant base vectors at time points t_{01}, t_{n1}, t_{02}, and t_{n2} were calculated to determine the corresponding metric tensors and the resulting Euler-Almansi strain tensors for beats 1 and 2. The direction defined by the belly markers 9 and 11 (Figure 1B) in the deformed configuration, ie, at times t_{n1} and t_{n2} for beat 1 and beat 2, respectively, was interpreted as the circumferential direction. The radial direction was defined orthogonal to the circumferential axis, passing through belly marker 10 (see Figure 1B). The largest projections of the Euler-Almansi strain tensor onto the circumferential and radial directions were defined as global maximum circumferential strain (global ε_{cir}) and global maximum radial strain (global ε_{rad}), respectively. These values were determined for 2 beats in each animal and each state (with and without annuloplasty device implanted). The animal global maximum principal strain (global ε_{max}) was calculated as the 2-beat average for each animal and each state by solving the eigenvalue problem for the Euler-Almansi strain tensor.

Maximum Principal (ε_{max},), Radial (ε_{rad}), and Circumferential (ε_{cir}) Strains Across the Entire AML

To provide a qualitative description of changes in strain patterns across the entire AML with and without annuloplasty device implanted, the 2-beat averages of ε_{max}, ε_{rad}, and ε_{cir} values of each triangular element were calculated for each animal in each state. These values were averaged for all animals (by extrapolating constant average element strains to the individual marker positions using superconvergent patch recovery to obtain smoothly varying strain profiles) and plotted onto color-mapped schematics.

Statistical Analysis

Average values of all animals in the respective groups were reported as mean±1 SD. All data reported for individual animals and all data used for quantitative statistical comparisons are 2-beat averages. Data with and without annuloplasty ring (or band) were compared using 1-way repeated-measures analysis of variance with a Holm-Sidak post hoc test (Sigmaplot 11.0, Systat Software Inc). To look at strain differences between the ring groups, maximum principal (ε_{max},), radial (ε_{rad}), and circumferential (ε_{cir}) strains with rings (COS, RSAR, PHYSIO, ETL, and GEO) were compared using 1-way analysis of variance. A probability value of less than 0.05 was considered statistically significant.

Results

Heart Rate, Left Ventricular End-Diastolic Volume, and dP/dt_{max}

Group mean heart rates, left ventricular end-diastolic volumes, and dP/dt_{max} are shown in Table 1. No significant differences were found between ring and control states in all 5 groups (except for Cosgrove, where dP/dt_{max} was slightly higher compared with control).

Left Ventricular Pressures and Volumes at Reference State (t_0) and Deformed State (t_n)

Table 2 shows LVPs and LVVs at t_0 and t_n, as well as Δ_{LVP} and Δ_{LVV}. Δ_{LVP} and Δ_{LVV} are also graphically depicted in Figure 3 (top row). A significant increase in LVPs by approximately 80mmHg (note that changes in LVP and LVV (Δ_{LVP} and Δ_{LVV}) are described from t_0 to t_n, ie, backward in time) occurred in both ring and control states from t_0 to t_n, whereas no relevant LVV changes were observed.

Mitral Annular Dimensions at Reference State (t_0) and Deformed State (t_n)

Table 3 shows the mitral annular S-L and C-C dimensions at t_n and t_0, as well as $\Delta_{S\text{-}L}$ and $\Delta_{C\text{-}C}$. $\Delta_{S\text{-}L}$ and $\Delta_{C\text{-}C}$ are also graphically depicted in Figure 3 (middle row). Again, note

Table 2. Left Ventricular Pressures and Volumes at Reference State (t_0) and Strained State (t_n)

	Animal No												Mean±1SD											
													LVP (mm Hg)						LVV (mL)					
	1	2	3	4	5	6	7	8	9	10	11	12	t_0	*P* vs CTRL	t_n	*P* vs CTRL	Δ_{tn-t0}	*P* vs CTRL	t_0	*P* vs CTRL	t_n	*P* vs CTRL	Δ_{tn-t0}	*P* vs CTRL
COS-CTRL																								
LVP (mm Hg)																								
t_0	20	10	45	17	24	12	15	9	7	6	18	7	16±11											
t_n	87	97	82	105	109	100	95	87	103	94	88	103			96±8									
Δ_{tn-t0}	68	88	37	89	85	88	79	78	96	88	69	96					80±16							
LVV (mL)																								
t_0	87	78	88	122	94	81	86	72	91	102	108	99							92±14					
t_n	91	85	89	124	97	82	92	80	92	101	112	102									96±13			
Δ_{tn-t0}	4.1	6.7	1.1	1.6	3.7	1.8	6.1	7.6	0.9	−0.6	4.0	3.0											3.3±2.5	
COS																								
LVP (mm Hg)																								
t_0	13	10	18	17	24	17	15	10	5	2	12	6	12±6	0.188										
t_n	90	99	90	100	109	107	98	91	100	97	92	97			97±6	0.218								
Δ_{tn-t0}	77	89	71	84	85	90	83	81	94	95	81	91					85±7	0.132						
LVV (mL)																								
t_0	90	76	101	126	89	81	80	72	87	101	109	97							92±15	0.940				
t_n	93	81	102	126	94	85	88	80	88	101	116	99									96±14	0.708		
Δ_{tn-t0}	3.6	5.6	0.8	0.6	4.4	3.9	8.0	7.6	0.9	−0.1	7.3	2.2											3.7±2.9	0.323
RSAR-CTRL																								
LVP (mm Hg)																								
t_0	39	4	12	21	11	15	25	19	14	7	17	14	16±9											
t_n	100	96	101	91	97	125	107	107	95	98	95	96			101±9									
Δ_{tn-t0}	61	92	89	71	86	109	82	87	80	91	78	82					84±12							
LVV (mL)																								
t_0	75	63	113	77	83	81	109	113	90	102	103	101							92±17					
t_n	74	68	120	79	93	89	113	117	94	108	106	106									97±17			
Δ_{tn-t0}	−1.1	5.7	6.6	1.7	10.3	8.4	3.5	3.7	4.3	6.2	2.9	4.6											4.7±3.0	

(*Continued*)

Table 2. Continued

	Animal No												Mean±1SD											
													LVP (mm Hg)						LVV (mL)					
	1	2	3	4	5	6	7	8	9	10	11	12	t_0	*P* vs CTRL	t_n	*P* vs CTRL	Δ_{tn-t0}	*P* vs CTRL	t_0	*P* vs CTRL	t_n	*P* vs CTRL	Δ_{tn-t0}	*P* vs CTRL
RSAR																								
LVP (mm Hg)																								
t_0	33	7	10	21	10	13	18	18	13	7	8	11	14±7	0.040										
t_n	92	91	102	95	102	109	95	101	95	97	94	98			98±5	0.144								
Δ_{tn-t0}	59	83	92	75	92	96	77	82	83	90	86	87					83±10	0.752						
LVV (mL)																								
t_0	75	67	120	81	85	81	110	115	88	102	102	103							94±17	0.027				
t_n	75	75	124	83	95	89	114	121	92	107	107	107									99±17	0.022		
Δ_{tn-t0}	−0.2	7.9	4.1	2.4	10.7	7.5	3.5	6.0	4.0	4.8	5.4	3.5											5.0±2.9	0.639
PHYSIO-CTRL																								
LVP (mm Hg)																								
t_0	32	2	24	6	13	41	33	5	2	37	10	12	18±14											
t_n	95	81	85	83	108	97	95	96	101	101	95	97			95±8									
Δ_{tn-t0}	63	79	61	77	95	56	62	91	99	64	85	85					76±15							
LVV (mL)																								
t_0	123	102	94	113	96	72	88	95	66	105	93	97							95±16					
t_n	122	109	94	116	98	69	88	100	70	100	95	102									97±16			
Δ_{tn-t0}	−1.1	6.4	−0.1	2.7	1.5	−2.2	−0.1	5.6	4.1	−4.5	2.2	4.4											1.6±3.3	
PHYSIO																								
LVP (mm Hg)																								
t_0	28	2	26	4	7	46	29	3	2	33	11	8	17±15	0.124										
t_n	97	83	86	87	103	98	97	96	95	99	99	97			95±6	0.949								
Δ_{tn-t0}	69	81	60	83	96	52	67	93	92	65	89	89					78±15	0.221						
LVV (mL)																								
t_0	123	107	97	119	95	62	87	98	71	105	97	99							97±17	0.285				
t_n	123	112	100	122	95	61	87	100	75	102	101	103									98±18	0.236		
Δ_{tn-t0}	−0.6	5.8	3.4	3.4	0.4	−1.6	0.4	1.9	4.1	−2.8	3.4	3.8											1.8±2.6	0.657

(*Continued*)

Table 2. Continued

	Animal No												Mean±1SD											
													LVP (mm Hg)						LVV (mL)					
	1	2	3	4	5	6	7	8	9	10	11	12	t_0	*P* vs CTRL	t_n	*P* vs CTRL	Δ_{tn-t0}	*P* vs CTRL	t_0	*P* vs CTRL	t_n	*P* vs CTRL	Δ_{tn-t0}	*P* vs CTRL
ETL-CTRL																								
LVP (mm Hg)																								
t_0	10	19	10	15	17	13	15	11	14	11	21		14±4											
t_n	95	93	98	92	90	89	105	91	91	98	103				95±5									
Δ_{tn-t0}	85	74	88	77	73	75	89	80	77	86	81						81±6							
LVV (mL)																								
t_0	96	87	64	110	87	68	90	104	104	107	110								93±16					
t_n	123	89	77	115	95	70	91	112	105	115	120										101±18			
Δ_{tn-t0}	26.9	2.1	12.3	5.6	8.0	2.9	0.9	7.5	0.7	7.1	9.2												7.6±7.4	
ETL																								
LVP (mm Hg)																								
t_0	11	11	8	9	13	12	13	10	12	12	15		11±2	0.010										
t_n	98	93	103	90	93	94	101	95	94	98	98				96±4	0.306								
Δ_{tn-t0}	87	82	95	80	79	82	88	85	83	87	83						85±4	0.080						
LVV (mL)																								
t_0	97	91	66	114	93	72	89	106	107	104	115								96±16	0.015				
t_n	123	94	77	115	101	74	91	114	106	113	122										103±17	0.034		
Δ_{tn-t0}	25.2	2.7	11.0	1.6	7.7	2.2	1.8	8.1	−1.2	9.1	6.8												6.8±7.2	0.186
GEO-CTRL																								
LVP (mm Hg)																								
t_0	18	13	33	16	17	8	11	1	3	3	3	15	12±9											
t_n	98	91	100	111	105	105	86	96	96	88	93	88			96±8									
Δ_{tn-t0}	81	77	67	95	88	98	75	95	93	85	90	72					85±10							
LVV (mL)																								
t_0	70	74	99	86	102	118	99	84	88	75	81	90							89±14					
t_n	77	88	103	93	99	125	101	92	90	74	85	99									94±14			
Δ_{tn-t0}	7.0	14.0	4.1	7.7	−3.9	7.8	2.3	7.8	2.4	−1.0	3.6	9.0											5.1±4.8	

(*Continued*)

Table 2. Continued

	Animal No												Mean±1SD											
													LVP (mm Hg)						LVV (mL)					
	1	2	3	4	5	6	7	8	9	10	11	12	t_0	*P* vs CTRL	t_n	*P* vs CTRL	Δ_{tn-t0}	*P* vs CTRL	t_0	*P* vs CTRL	t_n	*P* vs CTRL	Δ_{tn-t0}	*P* vs CTRL
GEO																								
LVP (mm Hg)																								
t_0	17	10	24	15	14	8	8	1	2	7	6	8	10±6	0.175										
t_n	93	90	96	110	101	111	92	96	99	92	96	88			97±7	0.589								
Δ_{tn-t0}	76	81	73	95	87	103	83	95	97	85	90	81					87±9	0.088						
LVV (mL)																								
t_0	74	77	102	86	98	122	98	83	91	92	82	91							91±13	0.131				
t_n	78	92	105	92	97	130	101	90	91	78	82	102									95±14	0.289		
Δ_{tn-t0}	4.0	14.6	2.6	6.1	−1.6	7.9	2.5	7.0	0.6	−14.7	0.7	10.6											3.4±7.3	0.175

All values from individual animals are 2-beat averages. t_n=strained state (time point of maximum LVP); t_0=reference strain state (time point before mitral valve opening; see Methods). COS indicates Cosgrove-Edwards band; CTRL, control; ETL, Edwards IMR ETlogix; GEO, Edwards GeoForm; LVP, left ventricular pressure; LVV, left ventricular volume; PHYSIO, Carpentier-Edwards Physio; RSAR, Saint Jude Medical rigid saddle-shaped annuloplasty ring.

that $\Delta_{S\text{-}L}$ and $\Delta_{C\text{-}C}$ are described from t_0 to t_n, ie, backward in time. Consequently, negative $\Delta_{S\text{-}L}$ and $\Delta_{C\text{-}C}$ represent an increase, whereas positive $\Delta_{S\text{-}L}$ and $\Delta_{C\text{-}C}$ represent a decrease in the respective dimension during the regular cardiac cycle. Relative to control, implantation of either complete, rigid rings (RSAR, PHYSIO, ETL, or GEO) or the flexible band (COS) resulted in significantly smaller mitral annular S-L and C-C dimensions. Decreases in S-L and C-C diameters from t_0 to t_n (negative $\Delta_{S\text{-}L}$ and $\Delta_{C\text{-}C}$, Table 3) were observed for the control cases (all groups). With the annuloplasty device implanted, the S-L dimension became slightly smaller from t_0 to t_n with COS ($\Delta_{S\text{-}L}$: −0.9±0.5 mm, Table 3 and Figure 3, middle row), whereas no relevant decreases in S-L and C-C diameters from t_0 to t_n were found with RSAR, PHYSIO, ETL, or GEO.

Global Maximum Principal (Global ε_{max}), Radial (global ε_{rad}), and Circumferential (Global ε_{cir}) Strains

Table 4 shows global ε_{max}, ε_{rad}, and ε_{cir} for all 5 groups with and without annuloplasty devices implanted. Global ε_{max}, ε_{rad}, and ε_{cir} (average from all animals) are also graphically displayed in Figure 3 (bottom row). Compared with the respective control state, strains increased significantly with RSAR, PHYSIO, ETL, and GEO (0.14±0.05 versus 0.16±0.05, P=0.024; 0.15±0.03 versus 0.18±0.04, P=0.020; 0.11±0.05 versus 0.14±0.05, P=0.042; and 0.13±0.05 versus 0.16±0.05, P=0.009, respectively; all P<0.05), but not with COS (0.15±0.05 versus 0.15±0.04, not significant, P=0.973). Global ε_{rad} increased significantly compared with the control state only with RSAR, whereas greater global ε_{cir} values were found with RSAR, PHYSIO, ETL, and GEO (however, they were insignificant for GEO; Table 4). No significant changes in global ε_{rad} or ε_{cir} were found with COS compared with the control state. With no annuloplasty device implanted, global ε_{rad} was greater than global ε_{cir} in all 5 groups (COS-CTRL, RSAR-CTRL, PHYSIO-CTRL, ETL-CTRL, GEO-CTRL; Table 4 and Figure 3, bottom row). With the annuloplasty device implanted, global ε_{rad} values were either greater than global ε_{cir} (COS, RSAR), smaller (PHYSIO), or similar (ETL, GEO; Table 4 and Figure 3, bottom row). No differences in ε_{max} (P=0.331, F=1.178), ε_{rad} (P=0.188, F=1.598), or ε_{cir} (P=0.160, F=1.716) with rings implanted were found between the groups (COS, RSAR, PHYSIO, ETL, and GEO).

Maximum Principal, Radial, and Circumferential Strains Across the Entire AML

Figure 4 shows maximum principal (ε_{max}), radial (ε_{rad}), and circumferential (ε_{cir}) strains across the entire AML for both states, with and without annuloplasty device implanted in all 5 groups. Increases in ε_{max} can be appreciated with RSAR, PHYSIO, ETL, and GEO compared with the respective control state and predominantly occur in the belly and edge region of the AML. No major changes in strain patterns (ε_{max}, ε_{rad}, or ε_{cir}) were observed with COS. ε_{max} values across the AML of the respective control states were slightly different between groups, with COS-CTRL, RSAR-CTRL, and

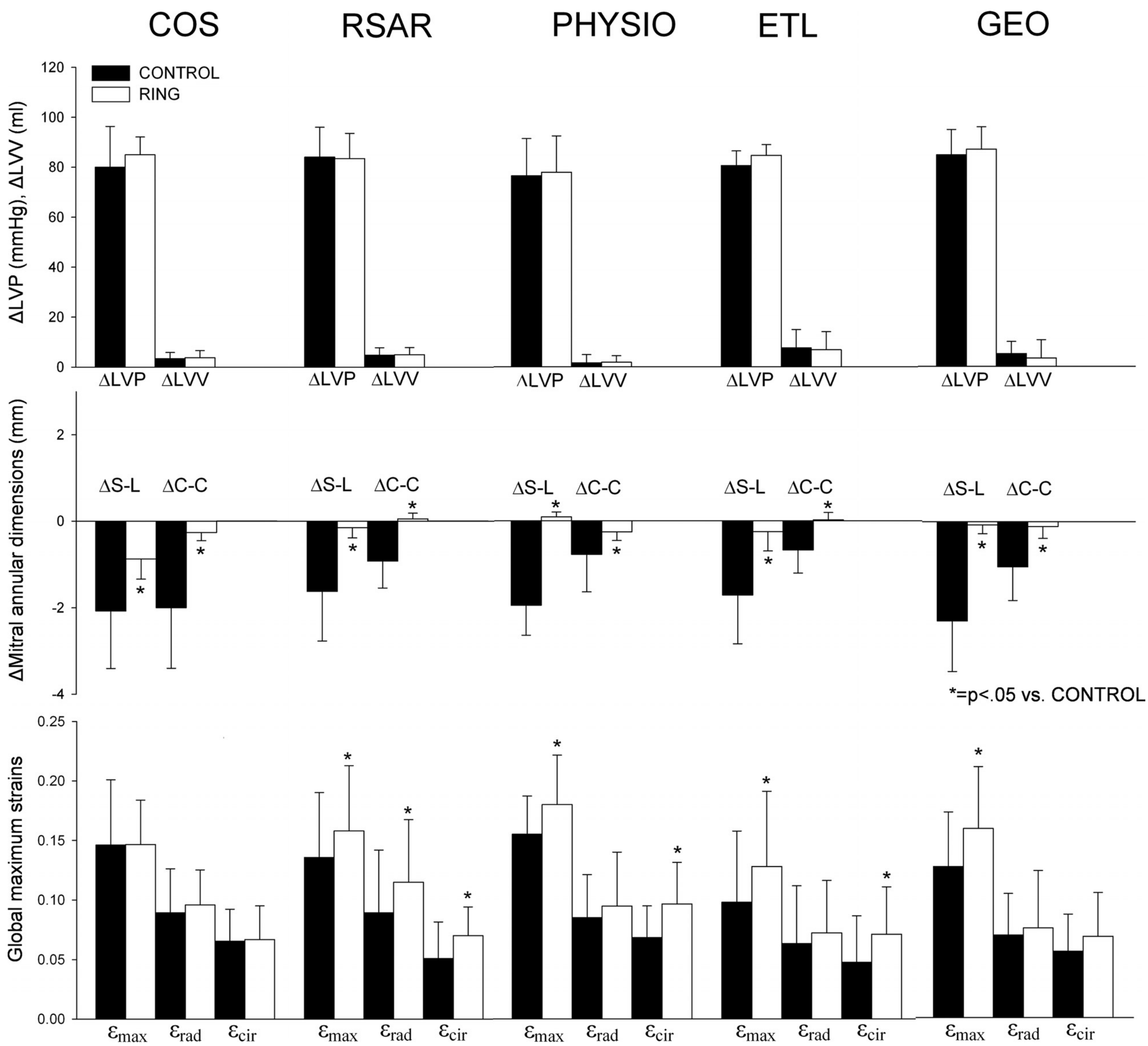

Figure 3. Changes in left ventricular pressure (Δ_{LVP}) and left ventricular volume (Δ_{LVV}) (top row), changes in mitral annular dimensions from reference state (t_0) to strained state (t_n) (middle row), and changes in global maximum principal (ε_{max}), radial (ε_{rad}), and circumferential (ε_{cir}) strains (bottom row). Note that changes from t_0 to t_n include a calculation from a time point later in the cardiac cycle (t_0) to an earlier time point of the cardiac cycle (t_n) (see Methods for definition of t_0 and t_n). C-C indicates commissure-commissure; COS, Cosgrove-Edwards band; ETL, Edwards IMR ETlogix; GEO, Edwards GeoForm; PHYSIO, Carpentier-Edwards Physio; RSAR, St Jude Medical rigid saddle-shaped annuloplasty ring; S-L, septal-lateral. Values are mean±1 SD.

PHYSIO-CTRL being more strained than GEO-CTRL and ETL-CTRL.

Discussion

The principal finding of this study was that with no relevant changes in hemodynamics, implantation of rigid, complete annuloplasty rings (RSAR, PHYSIO, ETL, and GEO), but not of the flexible, partial band (COS), increased global maximum principal strains of the AML. These changes occurred predominantly in the region of the AML belly and edge.

Several studies have determined mitral leaflet strains and stretches using a variety of different techniques.[4–7,14–19] In vitro studies have been used to characterize dynamic stretches on the anterior and posterior leaflet of excised porcine mitral valves using a left heart simulator.[6,14–17] In vivo studies, using sonomicrometer technology, quantified AML strains in the beating ovine heart,[16] and lastly, finite element studies investigated strain patterns across the AML.[4,5,18,19]

Salgo et al demonstrated in a numeric simulation that the native mitral annular shape is important to minimize stresses acting on the leaflet.[5] In a previous analysis from the same data set, we demonstrated that implantation of the PHYSIO, IMR ETL, and GEO, but not RSAR, perturbed the physiological saddle shape of the mitral annulus.[11] The increased maximum principal leaflet strains observed with these 3 rings are therefore consistent with engineering intuition quantified through the results of Salgo et al.[5] However, to our surprise, the supposedly physiologically shaped RSAR also led to an increase in maximum principal leaflet strains. Assuming that

Table 3. Mitral Annular Septal-Lateral and Commissure-Commissure Dimensions at Reference State (t_0) and Strained State (t_n)

	Animal No												Mean±1 SD											
													S−L						C−C					
	1	2	3	4	5	6	7	8	9	10	11	12	t_0	*P* vs CTRL	t_n	*P* vs CTRL	Δ_{tn-t0}	*P* vs CTRL	t_0	*P* vs CTRL	t_n	*P* vs CTRL	Δ_{tn-t0}	*P* vs CTRL
COS-CTRL																								
S−L																								
t_0	29.3	29.9	27.2	33.2	27.2	24.6	32.7	28.8	27.1	25.9	35.7	29.8	29.3±3.3											
t_n	27.9	27.4	26.3	28.7	23.0	22.7	30.5	27.5	24.9	26.1	34.6	26.9			27.2±3.2									
Δ_{tn-t0}	−1.4	−2.4	−1.0	−4.5	−4.2	−1.9	−2.2	−1.3	−2.2	0.2	−1.1	−2.9					−2.1±1.3							
C−C																								
t_0	36.2	36.9	34.6	37.2	36.9	33.8	40.4	41.6	42.4	36.5	38.9	39.0							37.8±2.7					
t_n	35.7	36.2	34.1	36.3	34.1	33.1	39.8	40.6	40.8	35.7	38.0	37.9									36.8±2.6			
Δ_{tn-t0}	−0.4	−0.7	−0.5	−1.0	−2.8	−0.7	−0.6	−1.0	−1.6	−0.8	−0.9	−1.1											−1.0±0.6	
COS																								
S−L																								
t_0	23.5	26.1	26.0	29.7	23.9	24.2	30.6	25.9	24.5	26.1	32.2	27.5	26.7±2.8	<0.001										
t_n	22.9	25.5	25.2	29.1	22.5	22.9	28.9	25.7	23.7	25.5	31.8	26.2			25.8±2.8	0.008								
Δ_{tn-t0}	−0.6	−0.6	−0.9	−0.6	−1.5	−1.3	−1.7	−0.2	−0.7	−0.6	−0.4	−1.3					−0.9±0.5	0.006						
C−C																								
t_0	30.6	32.7	32.0	34.6	32.6	33.6	38.3	38.8	38.0	35.9	35.2	37.9							35.0±2.8	0.004				
t_n	30.4	32.6	31.7	34.4	32.3	33.4	38.1	38.3	38.1	35.2	34.8	37.6									34.7±2.8	0.001		
Δ_{tn-t0}	−0.3	0.0	−0.3	−0.1	−0.3	−0.2	−0.2	−0.5	0.0	−0.7	−0.4	−0.3											−0.3±0.2	0.002
RSAR-CTRL																								
S−L																								
t_0	30.5	23.3	27.5	27.3	27.6	29.7	29.1	30.8	27.5	33.9	28.5	30.4	28.8±2.6											
t_n	30.0	22.9	26.4	27.3	25.9	28.3	27.7	27.1	25.3	30.5	26.6	28.7			27.2±2.1									
Δ_{tn-t0}	−0.5	−0.3	−1.1	0.0	−1.7	−1.4	−1.4	−3.8	−2.2	−3.5	−1.9	−1.7					−1.6±1.1							
C−C																								
t_0	37.6	32.7	32.9	35.2	37.7	35.6	36.4	40.1	36.7	42.1	38.6	40.4							37.2±2.9					
t_n	36.6	32.5	32.5	34.7	36.3	34.1	35.5	38.0	36.7	41.1	37.3	40.0									36.3±2.7			
Δ_{tn-t0}	−1.1	−0.2	−0.5	−0.5	−1.4	−1.6	−0.9	−2.2	0.0	−1.0	−1.3	−0.5											−0.9±0.6	

(Continued)

Table 3. Continued

	Animal No												Mean±1 SD											
													S−L						C−C					
	1	2	3	4	5	6	7	8	9	10	11	12	t_0	*P* vs CTRL	t_n	*P* vs CTRL	Δ_{tn-t0}	*P* vs CTRL	t_0	*P* vs CTRL	t_n	*P* vs CTRL	Δ_{tn-t0}	*P* vs CTRL
RSAR																								
S−L																								
t_0	25.4	23.7	24.9	24.1	24.6	25.8	24.8	25.0	23.5	26.5	24.7	24.6	24.8±0.8	<0.001										
t_n	25.2	24.0	24.6	23.9	24.5	25.7	24.6	24.9	22.9	26.4	24.8	24.4			24.6±0.9	<0.001								
Δ_{tn-t0}	−0.2	0.3	−0.3	−0.3	−0.1	−0.1	−0.2	−0.2	−0.6	−0.1	0.1	−0.2					−0.2±0.2	0.001						
C−C																								
t_0	34.5	33.4	33.7	33.8	33.8	34.6	34.3	33.1	31.1	33.0	31.8	33.8							33.4±1.0	0.009				
t_n	34.3	33.6	33.7	33.8	33.8	34.5	34.5	33.4	31.3	33.1	31.8	33.9									33.5±1.0	0.002		
Δ_{tn-t0}	−0.2	0.2	0.0	0.0	0.0	−0.1	0.2	0.3	0.1	0.1	−0.1	0.0											0.1±0.1	<0.001
PHYSIO-CTRL																								
S−L																								
t_0	30.1	26.9	26.5	30.5	27.7	25.3	30.5	35.6	27.7	31.2	33.1	30.2	29.6±3.0											
t_n	28.6	26.1	24.0	27.6	25.7	24.5	28.4	33.5	25.2	29.6	31.4	27.3			27.7±2.9									
Δ_{tn-t0}	−1.5	−0.9	−2.4	−2.9	−2.0	−0.8	−2.1	−2.1	−2.5	−1.7	−1.7	−3.0					−2.0±0.7							
C−C																								
t_0	42.6	37.7	39.0	42.0	40.5	36.7	40.0	43.6	38.9	37.9	40.5	39.6							39.9±2.1					
t_n	41.2	39.1	37.5	41.4	39.9	35.7	39.4	43.2	37.1	37.9	39.3	38.4									39.1±2.1			
Δ_{tn-t0}	−1.4	1.4	−1.6	−0.6	−0.6	−1.1	−0.6	−0.4	−1.9	0.0	−1.2	−1.3											−0.8±0.9	
PHYSIO																								
S−L																								
t_0	24.2	24.2	24.6	24.1	23.5	23.3	25.0	28.1	24.1	26.1	25.9	26.1	24.9±1.4	<0.001										
t_n	23.9	24.0	24.2	23.8	22.8	23.1	24.6	28.2	23.8	25.9	25.9	25.9			24.7±1.5	<0.001								
Δ_{tn-t0}	−0.2	−0.2	−0.4	−0.2	−0.7	−0.2	−0.4	0.1	−0.4	−0.2	0.0	−0.3					−0.3±0.2	<0.001						
C−C																								
t_0	33.0	33.1	32.7	34.9	32.8	32.7	32.7	33.7	32.7	32.6	31.5	32.6							32.9±0.8	<0.001				
t_n	33.1	33.1	32.7	34.8	32.8	32.6	32.8	33.9	32.9	32.9	31.7	32.9									33.0±0.8	<0.001		
Δ_{tn-t0}	0.0	0.0	0.0	−0.1	0.1	−0.1	0.2	0.1	0.1	0.2	0.2	0.3											0.1±0.1	0.007

(*Continued*)

Table 3. Continued

	Animal No												Mean±1 SD											
													S−L						C−C					
	1	2	3	4	5	6	7	8	9	10	11	12	t_0	*P* vs CTRL	t_n	*P* vs CTRL	Δ_{tn-t0}	*P* vs CTRL	t_0	*P* vs CTRL	t_n	*P* vs CTRL	Δ_{tn-t0}	*P* vs CTRL
ETL-CTRL																								
S−L																								
t_0	29.2	32.1	28.0	27.5	29.8	26.2	33.3	32.6	32.6	30.6	28.7		30.1±2.4											
t_n	27.9	31.4	24.8	25.8	27.9	27.1	31.1	30.5	31.1	27.5	27.0				28.4±2.3									
Δ_{tn-t0}	−1.3	−0.7	−3.3	−1.7	−1.9	0.9	−2.3	−2.1	−1.6	−3.1	−1.7						−1.7±1.1							
C−C																								
t_0	34.0	39.8	35.6	39.6	40.4	43.6	36.8	38.8	41.0	40.7	41.5								39.2±2.8					
t_n	34.0	39.0	35.4	38.3	39.5	43.0	36.6	38.3	40.8	39.7	39.8										38.6±2.5			
Δ_{tn-t0}	0.0	−0.7	−0.2	−1.3	−1.0	−0.7	−0.2	−0.5	−0.2	−1.0	−1.7												−0.7±0.5	
ETL																								
S−L																								
t_0	23.1	25.5	20.7	24.5	24.3	21.0	22.9	24.2	24.1	24.2	23.5		23.4±1.5	<0.001										
t_n	23.6	25.3	20.5	23.1	23.9	20.8	22.7	23.9	24.0	24.0	23.1				23.2±1.4	<0.001								
Δ_{tn-t0}	0.5	−0.1	−0.2	−1.3	−0.4	−0.1	−0.2	−0.4	−0.1	−0.2	−0.4						−0.3±0.4	0.002						
C−C																								
t_0	29.0	32.3	29.9	30.6	33.3	33.9	32.3	33.2	32.8	32.7	32.7								32.1±1.5	<0.001				
t_n	29.3	32.2	30.1	30.8	33.0	33.9	32.5	33.1	32.7	32.7	32.7										32.1±1.4	<0.001		
Δ_{tn-t0}	0.3	−0.1	0.2	0.2	−0.2	0.0	0.2	−0.1	−0.2	0.1	0.0												0.0±0.2	0.001
GEO-CTRL																								
S−L																								
t_0	27.6	29.8	26.0	29.8	27.5	27.2	31.1	29.6	30.9	28.3	24.8	30.1	28.6±2.0											
t_n	25.8	28.5	25.2	27.9	23.5	23.2	29.0	26.6	27.0	27.6	22.8	28.1			26.3±2.2									
Δ_{tn-t0}	−1.8	−1.3	−0.9	−1.9	−4.1	−4.0	−2.2	−2.9	−3.9	−0.7	−2.0	−2.0					−2.3±1.2							
C−C																								
t_0	36.6	34.8	34.2	35.7	36.6	36.8	38.3	38.5	42.5	41.0	37.4	43.0							37.9±2.9					
t_n	35.1	35.2	33.2	34.9	33.9	36.2	37.9	37.8	40.4	40.0	36.4	41.7									36.9±2.7			
Δ_{tn-t0}	−1.5	0.4	−1.0	−0.8	−2.6	−0.6	−0.4	−0.7	−2.1	−0.9	−1.0	−1.3											−1.0±0.8	

(*Continued*)

Table 3. Continued

	Animal No												Mean±1 SD											
													S−L						C−C					
	1	2	3	4	5	6	7	8	9	10	11	12	t_0	P vs CTRL	t_n	P vs CTRL	Δ_{tn-t0}	P vs CTRL	t_0	P vs CTRL	t_n	P vs CTRL	Δ_{tn-t0}	P vs CTRL
GEO																								
S−L																								
t_0	19.9	19.6	19.6	20.6	19.7	19.1	21.0	20.7	21.6	18.7	18.7	19.7	19.9±0.9	<0.001										
t_n	19.8	19.8	19.5	20.7	19.5	18.9	21.1	20.5	21.1	18.7	18.9	19.7			19.8±0.8	<0.001								
Δ_{tn-t0}	−0.1	0.2	−0.1	0.2	−0.3	−0.2	0.1	−0.2	−0.5	−0.1	0.2	−0.1					−0.1±0.2	<0.001						
C−C																								
t_0	33.4	33.4	31.5	34.9	34.8	33.7	35.8	36.5	35.7	35.4	35.7	36.2							34.7±1.5	0.001				
t_n	33.2	33.7	31.4	34.7	34.1	33.3	36.1	36.4	35.7	35.3	35.6	36.1									34.6±1.5	<0.001		
Δ_{tn-t0}	−0.2	0.3	−0.1	−0.2	−0.7	−0.4	0.3	−0.1	0.0	0.0	−0.1	−0.1											−0.1±0.3	<0.001

All values from individual animals are in mm and 2-beat averages. t_n=strained state (time point of maximum left ventricular pressure); t_0=reference strain state (time point before mitral valve opening; see Methods). C-C indicates commissure-commissure; COS, Cosgrove-Edwards band; CTRL, control; ETL, Edwards IMR ETlogix; GEO, Edwards GeoForm; PHYSIO, Carpentier-Edwards Physio; RSAR, Saint Jude Medical rigid saddle-shaped annuloplasty ring; S-L, septal-lateral.

the shape of this ring is physiological, it could be speculated that the dynamic motion of the mitral annulus, rather than its 3D shape, is of major importance to preserve AML strain distribution. This hypothesis, however, is contrary to previous studies that suggested changes in the physiological mitral annular 3D saddle shape lead to increases in leaflet strains.[6] It may therefore also be speculated that the shape of the RSAR does not fully represent the natural 3D annular shape and that, as discussed earlier,[6] increased strains are also a result of a nonphysiological annular shape.

The partial, flexible band (COS) has been found to preserve the mitral annular saddle shape[11] and allow minimal mitral annular S-L dynamics (Figure 3, middle row) during the observed time period (from t_0 to t_n). However, COS significantly reduced mitral annular dimensions compared with the control state (Table 3 and Bothe et al[11]). Because COS did not affect AML strains (Figure 3, bottom row), we speculate that preserving physiological mitral annular dynamics and shape rather than absolute mitral annular dimensions are the key components to maintaining a physiological strain distribution across the AML.

To our knowledge, Votta et al are the only group that has quantified the effects of annuloplasty rings (GEO and PHYSIO) on mitral leaflet strains and stresses.[4] The group used a finite element model and demonstrated that the GEO, but not the PHYSIO, reduced maximum principal mitral leaflet stresses during simulated functional mitral regurgitation.[4] In our study, we found that all rigid rings (RSAR, PHYSIO, ETL, and GEO) increased maximum principal AML strains, irrespective of their 3D shape. However, unlike Votta et al, we used an in vivo model of the normal, beating heart. We therefore cannot comment on the potential effects of rings designed to treat functional or ischemic mitral regurgitation (ie, GEO, ETL) in the diseased state, and it is possible that these rings restore a physiological strain distribution in hearts with dilated left ventricles.

In this study, we report the effect of different annuloplasty devices on radial and circumferential strains. Whereas global ε_{rad} was only greater with RSAR, global ε_{cir} was greater with all rigid, complete rings (RSAR, PHYSIO, ETL, and GEO; Table 4) compared with the control state (insignificantly, however, for GEO), suggesting that rigid, complete annuloplasty devices affect circumferential strains more than radial strains. The reason for the insignificant increase in global ε_{cir} observed with GEO could be a result of the larger commissure to commissure dimension of this ring compared with RSAR, PHYSIO, or ETL,[3] suggesting that the physiological circumferential AML strain distribution is sensitive to the amount of mitral annular C-C decrease.

Study Limitations

Several limitations should be addressed to allow a better interpretation of these data. First, the data were acquired from open-chest, anesthetized ovine hearts with normal preoperative anatomy. Considerable caution must therefore be exercised when extrapolating these findings to the human heart. This is especially true for the GEO and IMR ETL rings, which were designed for patients with ischemic or functional mitral regurgitation (with distorted annular, leaflet, and ven-

Table 4. Global Maximum Principal (Global ϵ_{max}), Radial (Global ϵ_{rad}), and Circumferential (Global ϵ_{cir}) Strains

	Animal No												Mean±1 SD					
	1	2	3	4	5	6	7	8	9	10	11	12	Global ϵ_{max}	*P* vs CTRL	Global ϵ_{rad}	*P* vs CTRL	Global ϵ_{cir}	*P* vs CTRL
COS-CTRL																		
Global ϵ_{max}	0.08	0.20	0.06	0.12	0.14	0.22	0.19	0.15	0.11	0.23	0.11	0.16	0.15±0.05					
Global ϵ_{rad}	0.03	0.12	0.04	0.08	0.08	0.17	0.10	0.09	0.08	0.10	0.05	0.12			0.09±0.04			
Global ϵ_{cir}	0.04	0.11	0.04	0.05	0.07	0.08	0.07	0.09	0.04	0.07	0.03	0.10					0.07±0.03	
COS																		
Global ϵ_{max}	0.19	0.19	0.07	0.13	0.14	0.14	0.15	0.14	0.12	0.16	0.12	0.21	0.15±0.04	0.973				
Global ϵ_{rad}	0.08	0.15	0.05	0.10	0.11	0.11	0.06	0.09	0.09	0.13	0.07	0.12			0.10±0.03	0.425		
Global ϵ_{cir}	0.08	0.08	0.04	0.05	0.07	0.04	0.08	0.06	0.05	0.10	0.03	0.13					0.07±0.03	0.858
RSAR-CTRL																		
Global ϵ_{max}	0.08	0.19	0.24	0.08	0.18	0.09	0.17	0.16	0.08	0.14	0.07	0.14	0.14±0.05					
Global ϵ_{rad}	0.04	0.15	0.20	0.05	0.10	0.03	0.10	0.16	0.04	0.09	0.05	0.07			0.09±0.05			
Global ϵ_{cir}	0.03	0.13	0.07	0.02	0.06	0.04	0.04	0.05	0.03	0.06	0.02	0.07					0.05±0.03	
RSAR																		
Global ϵ_{max}	0.15	0.17	0.24	0.09	0.21	0.09	0.18	0.18	0.10	0.15	0.09	0.23	0.16±0.05	0.024				
Global ϵ_{rad}	0.12	0.15	0.20	0.06	0.12	0.06	0.15	0.17	0.03	0.10	0.06	0.16			0.11±0.05	0.010		
Global ϵ_{cir}	0.06	0.09	0.09	0.05	0.11	0.05	0.07	0.04	0.06	0.06	0.05	0.11					0.07±0.02	0.022
PHYSIO-CTRL																		
Global ϵ_{max}	0.17	0.15	0.19	0.20	0.17	0.12	0.16	0.14	0.18	0.09	0.11	0.17	0.15±0.03					
Global ϵ_{rad}	0.11	0.04	0.08	0.09	0.14	0.04	0.12	0.08	0.10	0.03	0.07	0.13			0.08±0.04			
Global ϵ_{cir}	0.05	0.11	0.11	0.09	0.07	0.08	0.06	0.07	0.03	0.03	0.05	0.07					0.07±0.03	
PHYSIO																		
Global ϵ_{max}	0.21	0.18	0.21	0.19	0.20	0.12	0.20	0.20	0.14	0.14	0.11	0.24	0.18±0.04	0.020				
Global ϵ_{rad}	0.14	0.03	0.10	0.13	0.14	0.04	0.14	0.11	0.09	0.04	0.05	0.13			0.09±0.05	0.102		
Global ϵ_{cir}	0.10	0.13	0.10	0.10	0.10	0.05	0.11	0.13	0.04	0.08	0.06	0.15					0.10±0.03	0.010
ETL-CTRL																		
Global ϵ_{max}	0.21	0.08	0.09	0.12	0.07	0.10	0.07	0.08	0.09	0.20	0.06		0.11±0.05					
Global ϵ_{rad}	0.15	0.07	0.06	0.11	0.02	0.04	0.04	0.07	0.03	0.15	0.03				0.07±0.05			
Global ϵ_{cir}	0.13	0.02	0.03	0.05	0.05	0.06	0.04	0.03	0.02	0.12	0.03						0.05±0.04	
ETL																		
Global ϵ_{max}	0.19	0.11	0.17	0.24	0.06	0.11	0.15	0.11	0.12	0.17	0.09		0.14±0.05	0.042				
Global ϵ_{rad}	0.10	0.08	0.08	0.17	0.03	0.03	0.05	0.10	0.07	0.11	0.06				0.08±0.04	0.349		
Global ϵ_{cir}	0.14	0.05	0.11	0.12	0.04	0.08	0.07	0.04	0.05	0.09	0.06						0.08±0.03	0.017
GEO-CTRL																		
Global ϵ_{max}	0.13	0.15	0.04	0.17	0.06	0.08	0.19	0.17	0.11	0.13	0.16	0.13	0.13±0.05					
Global ϵ_{rad}	0.08	0.10	0.02	0.12	0.02	0.03	0.08	0.11	0.06	0.09	0.06	0.07			0.07±0.03			
Global ϵ_{cir}	0.07	0.10	0.01	0.07	0.02	0.02	0.11	0.03	0.07	0.05	0.05	0.06					0.06±0.03	
GEO																		
Global ϵ_{max}	0.14	0.21	0.05	0.22	0.16	0.07	0.17	0.20	0.16	0.16	0.18	0.19	0.16±0.05	0.009				
Global ϵ_{rad}	0.07	0.15	0.01	0.12	0.09	0.04	0.05	0.14	0.07	0.05	0.00	0.11			0.07±0.05	0.581		
Global ϵ_{cir}	0.09	0.11	0.02	0.13	0.02	0.02	0.08	0.04	0.10	0.07	0.07	0.07					0.07±0.04	0.065

All values from individual animals are 2-beat averages. COS, Cosgrove-Edwards band; CTRL, control; ETL, Edwards IMR ETlogix; GEO, Edwards GeoForm; PHYSIO, Carpentier-Edwards Physio; RSAR, Saint Jude Medical rigid saddle-shaped annuloplasty ring.

tricular geometry and function). As mentioned above, if these rings are implanted in the setting of functional or ischemic mitral regurgitation, it could well be that they reduce (or restore physiological) leaflet strains, as demonstrated by Votta et al in a computer simulation.[4] In future analyses, we aim to use our experimental in vivo data to determine whether these 2 rings designed to treat functional or ischemic mitral regurgitation (GEO and ETL) are more efficient than conventional rings in terms of reducing leaflet strains during acute myocardial ischemia. Second, AML strains were quantified for only the isovolumetric relaxation phase of the cardiac cycle, and it could be that the rings affect strain

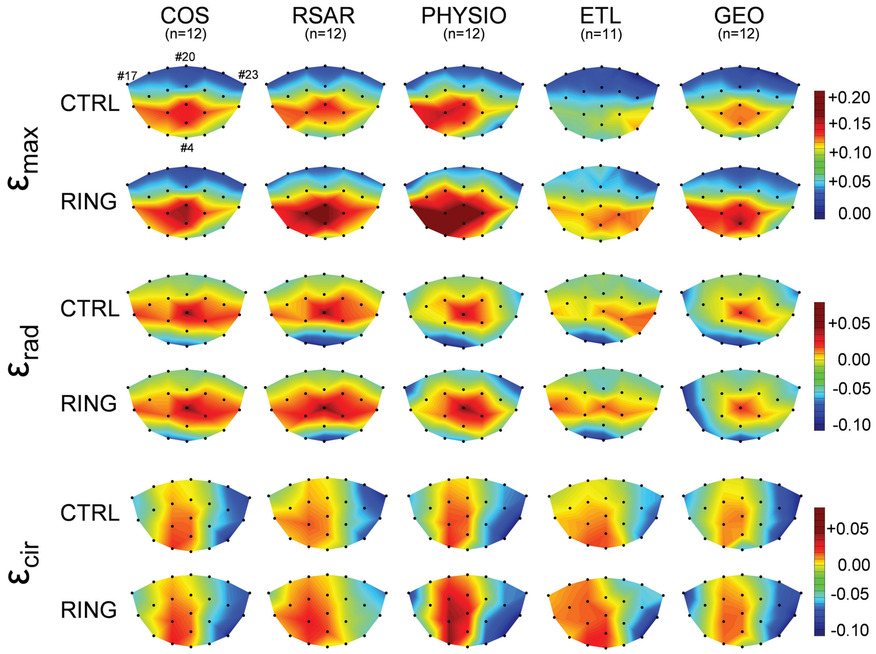

Figure 4. Color-mapped schematics of maximum principal (ε_{max}, 2 top rows), radial (ε_{rad}, 2 middle rows), and circumferential (ε_{cir}, 2 bottom rows) strains across the entire anterior mitral leaflet (AML) for the control state (CTRL) and with annuloplasty device implanted (RING). Markers 17 and 23 depict anterior and posterior commissures, respectively, and marker 20 represents the midseptal mitral annulus (saddle horn; see Figure 1). COS indicates Cosgrove-Edwards band; ETL, Edwards IMR ETlogix; GEO, Edwards GeoForm; PHYSIO, Carpentier-Edwards Physio; RSAR, St Jude Medical rigid saddle-shaped annuloplasty ring.

patterns differently in other phases of the cardiac cycle.[20] Third, although perturbed leaflet strains have been associated with impaired mitral valve repair durability,[6,7] currently no study exists that proves causation. Consequently, it remains to be determined whether perturbations in AML strains impair long-term function of the mitral valve after repair. Fourth, when radial and circumferential strains were plotted onto color-mapped schematics (Figure 4), we observed not only tensile but also compressive strains in both control states and with rings implanted (green and blue areas, Figure 4). Compressive strains do not occur, eg, in purely computational models that use simplified AML shapes with the leaflet being entirely convex to the left ventricle[4] and thus may be a result of the complex AML shape[21] that was included in our analyses. The finding of compressive strains warrants further investigation; however, in this study, we focused on the tensile aspects of strain and did not perform detailed analyses of compressive strain patterns. Fifth, no statistically significant differences in strains were found between the different ring types. We therefore cannot draw any conclusions from these data whether any ring design is superior to another; however, this study was not adequately powered to demonstrate differences between the different ring types. Sixth, we studied only a partial, flexible band. Because no complete, flexible ring was examined in this experiment, it is not possible to distinguish whether the observed lack of increase in AML strains with a partial band is due to its partial design, its flexibility, or a combination of the 2. Lastly, strain patterns may change with varying annuloplasty device sizes.[4] Because only 28-mm annuloplasty rings were used in this study, we are unable to draw any conclusions about the impact of ring or band size on leaflet strains.

Conclusions

In conclusion, regardless of their 3-dimensional shape, rigid, complete annuloplasty rings (RSAR, PHYSIO, ETL, GEO), but not a partial, flexible band (COS), increased maximum principal AML strains predominantly in the belly and edge regions in the normal beating ovine heart. Large, randomized clinical trials are needed to answer the question of whether the observed ring-induced alterations in mitral leaflet strain states exist in human patients, and if so, whether they adversely affect long-term mitral valve repair durability.

Acknowledgments

The authors gratefully acknowledge the expert technical assistance of Paul Chang, Maggie Brophy, Sigurd Hartnett, Erin Schultz, and George T. Daughters, as well as the inspiring suggestions of Frank Langer.

Sources of Funding

This study was funded by Research Grants R01-HL29589 (1982–2008) and R01-HL67025 (2001–2010), National Heart, Lung, and Blood Institute, National Institutes of Health (to D.C.M.); Research Grant S/06/07, Deutsche Herzstiftung, Frankfurt, Germany (to W.B.); National Science Foundation Career Award CMMI-0952021 (to E.K.); US-Norway Fulbright Foundation, the Swedish Heart-Lung Foundation, and the Swedish Society for Medical Research. (to J.-P.E.K.); and a Western States Affiliate American Heart Association Postdoctoral Fellowship (to J.C.S.).

Disclosures

Dr Miller is a consultant for Medtronic CardioVascular Division, St. Jude Medical, Inc, and Abbott Vascular (MitraClip) and a partner of the US Pivotal Trial Executive Committee and Edwards Lifesciences (uncompensated).

References

1. Ryan LP, Jackson BM, Hamamoto H, Eperjesi TJ, Plappert TJ, St John-Sutton M, Gorman RC, Gorman JH III. The influence of annuloplasty ring geometry on mitral leaflet curvature. *Ann Thorac Surg*. 2008;86:749–760, discussion 749–760.
2. Accola KD, Scott ML, Thompson PA, Palmer GJ III, Sand ME, Ebra G. Midterm outcomes using the physio ring in mitral valve reconstruction: experience in 492 patients. *Ann Thorac Surg*. 2005;79:1276–1283, discussion 1276–1283.

3. Bothe W, Swanson JC, Ingels NB, Miller DC. How much septal-lateral mitral annular reduction do you get with new ischemic/functional mitral regurgitation annuloplasty rings? *J Thorac Cardiovasc Surg*. 2010;140: 117–121, 121 e1–3.
4. Votta E, Maisano F, Bolling SF, Alfieri O, Montevecchi FM, Redaelli A. The Geoform disease-specific annuloplasty system: a finite element study. *Ann Thorac Surg*. 2007;84:92–101.
5. Salgo IS, Gorman JH III, Gorman RC, Jackson BM, Bowen FW, Plappert T, St John Sutton MG, Edmunds LH Jr. Effect of annular shape on leaflet curvature in reducing mitral leaflet stress. *Circulation*. 2002;106:711–717.
6. Jimenez JH, Liou SW, Padala M, He Z, Sacks M, Gorman RC, Gorman JH III, Yoganathan AP. A saddle-shaped annulus reduces systolic strain on the central region of the mitral valve anterior leaflet. *J Thorac Cardiovasc Surg*. 2007;134:1562–1568.
7. Padala M, Hutchison RA, Croft LR, Jimenez JH, Gorman RC, Gorman JH III, Sacks MS, Yoganathan AP. Saddle shape of the mitral annulus reduces systolic strains on the P2 segment of the posterior mitral leaflet. *Ann Thorac Surg*. 2009;88:1499–1504.
8. Bothe W, Chang PA, Swanson JC, Itoh A, Arata K, Ingels NB, Miller DC. Releasable annuloplasty ring insertion: a novel experimental implantation model. *Eur J Cardiothorac Surg*. 2009;36:830–832.
9. Bothe W, Kvitting JP, Stephens EH, Swanson JC, Liang DH, Ingels NB Jr, Miller DC. Effects of different annuloplasty ring types on mitral leaflet tenting area during acute myocardial ischemia. *J Thorac Cardiovasc Surg*. 2011;141:345–353.
10. Bothe W, Kvitting JP, Swanson JC, Goktepe S, Vo KN, Ingels NB, Miller DC. How do annuloplasty rings affect mitral leaflet dynamic motion? *Eur J Cardiothorac Surg*. 2010;38:340–349.
11. Bothe W, Kvitting JP, Swanson JC, Hartnett S, Ingels NB Jr, Miller DC. Effects of different annuloplasty rings on anterior mitral leaflet dimensions. *J Thorac Cardiovasc Surg*. 139:1114–1122.
12. Niczyporuk MA, Miller DC. Automatic tracking and digitization of multiple radiopaque myocardial markers. *Comput Biomed Res*. 1991;24: 129–142.
13. Moon MR, DeAnda A Jr, Daughters GT II, Ingels NB Jr, Miller DC. Experimental evaluation of different chordal preservation methods during mitral valve replacement. *Ann Thorac Surg*. 1994;58:931–943, discussion 943–944.
14. He Z, Sacks MS, Baijens L, Wanant S, Shah P, Yoganathan AP. Effects of papillary muscle position on in-vitro dynamic strain on the porcine mitral valve. *J Heart Valve Dis*. 2003;12:488–494.
15. He S, Jimenez J, He Z, Yoganathan AP. Mitral leaflet geometry perturbations with papillary muscle displacement and annular dilatation: an in-vitro study of ischemic mitral regurgitation. *J Heart Valve Dis*. 2003; 12:300–307.
16. Sacks MS, He Z, Baijens L, Wanant S, Shah P, Sugimoto H, Yoganathan AP. Surface strains in the anterior leaflet of the functioning mitral valve. *Ann Biomed Eng*. 2002;30:1281–1290.
17. Jimenez JH, Soerensen DD, He Z, He S, Yoganathan AP. Effects of a saddle shaped annulus on mitral valve function and chordal force distribution: an in vitro study. *Ann Biomed Eng*. 2003;31:1171–1181.
18. Kunzelman KS, Reimink MS, Cochran RP. Annular dilatation increases stress in the mitral valve and delays coaptation: a finite element computer model. *Cardiovasc Surg*. 1997;5:427–434.
19. Votta E, Maisano F, Soncini M, Redaelli A, Montevecchi FM, Alfieri O. 3-D computational analysis of the stress distribution on the leaflets after edge-to-edge repair of mitral regurgitation. *J Heart Valve Dis*. 2002;11: 810–822.
20. Itoh A, Krishnamurthy G, Swanson JC, Ennis DB, Bothe W, Kuhl E, Karlsson M, Davis LR, Miller DC, Ingels NB Jr. Active stiffening of mitral valve leaflets in the beating heart. *Am J Physiol Heart Circ Physiol*. 2009;296:H1766–73.
21. Ryan LP, Jackson BM, Eperjesi TJ, Plappert TJ, St John-Sutton M, Gorman RC, Gorman JH III. A methodology for assessing human mitral leaflet curvature using real-time 3-dimensional echocardiography. *J Thorac Cardiovasc Surg*. 2008;136:726–734.